Joint Design of Phase Shift and Transceiver Beamforming for Intelligent Reflecting Surface Assisted Millimeter-Wave High-speed Railway Communications

Chen Chen, Yong Niu, *Member, IEEE*, Bo Ai, *Fellow, IEEE*, Ruisi He, *Senior Member, IEEE*, Zhu Han, *Fellow, IEEE*, Zhangdui Zhong, *Fellow, IEEE*, Ning Wang, *Member, IEEE*, and Xiang Su, *Member, IEEE*

***Abstract*—With the emerging demands of new communication services, the contradiction between capacity demand and spectrum shortage of railway communication systems becomes more severe. How to provide broadband communication services has become the key goal of future smart high-speed railway (HSR) systems. Millimeter wave (mm-wave) frequency band has abundant spectrum resources and can provide communication services with large bandwidth. However, due to the high-speed of the train as well as the complexity and dynamics of environments, the communication link may be blocked randomly for a short time and will also lead to frequent handovers. In this paper, we adopt the promising intelligent reflecting surface (IRS) technology for a mm-wave HSR communication system. In order to improve system capacity, IRS is deployed to improve reflection transmission links, and optimization algorithms are designed for transceiver beamforming and IRS phase shift. In addition, given the specificity of the HSR scenario, we also formulate the average system ergodic capacity maximization problem and obtain upper bound on the average system ergodic capacity with statistical channel state information (CSI). Through extensive simulations, we verify that the proposed scheme performs significantly better than the other two baseline schemes in terms of average system throughput and average system ergodic capacity.**

***Index Terms*—High-speed railway, intelligent reconfigurable surface, millimeter-wave communications, phase shift, train-ground communications.**

I. Introduction

With boosting development of high-speed railway (HSR) worldwide, HSR has become the preferred mode of travel because of its advantages of fast speed, high safety and satisfied comfort. Take China's railways as an example, its operation length has reached nearly 39,000 km [1]. Moreover, since the passengers are accustomed to high quality services on the ground, they also demand to access the Internet during a long travel for working, studying and entertainment. Nevertheless, as the train runs at high speed, the relative rapid movement between the train and ground base station (BS) makes the wireless channel in HSR scenarios has obvious non-stationary and fast time-varying characteristics, which affect the overall performance of the HSR communication system [2]. In addition, frequent handovers occur in the HSR scenarios. Assuming that the speed of the train is 350 km/h and the radius of the cell is 1 to 2 km, handover occurs every 10 to 20s [1]. Therefore, the demand of data transmission with high capacity and large bandwidth for passengers in the carriage brings significant challenges to the HSR communication system. Obviously, it is important to carry out research on broadband wireless communication in HSR scenarios.

With the rapid emergence of new businesses and applications of "smart railway", the contradiction between capacity demand and spectrum shortage is becoming more and more obvious. Millimeter wave (mm-wave) frequency band covers from 30 GHz to 300 GHz and also has rich spectrum resources. It is expected to provide broadband access services of several Gbps transmission data rates for train-ground communication systems and reduce service delay. At present, mm-wave communications have made remarkable commercial progress in the world and have also been utilized in HSR systems. For example, the Shinkansen line in Japan, the Maglev train test line in Germany and the Maglev train in Shanghai [3] have all adopted the mm-wave communication technology. Research on mm-wave communication has also been recently carried out towards HSR communication systems.

However, since mm-wave communications face serious propagation loss and link attenuation, the research on HSR communication systems mainly adopt the two-hop communication system model assisted by mobile relay (MR), i.e., the two-hop data transmission link of communication outside the train and communication inside the train, which can effectively avoid serious penetration loss and frequent group handovers [4]. Therefore, we mainly focus on the mm-wave HSR communication system assisted by MR in this study. Also, it is crucial to use beamforming technology to obtain higher antenna gain [5] and compensate high attenuation during the signal transmission. In addition, the short wavelength of mm-wave leads to poor diffraction ability and is more vulnerable to the shelter of human body, trees and even buildings, which reduces the performance of receiving signals and even leads

C. Chen is with the State Key Laboratory of Rail Traffic Control and Safety, and also with the Frontiers Science Center for Smart High-speed Railway System, Beijing Jiaotong University, Beijing 100044, China (e-mail: 20120026@bjtu.edu.cn).

Y. Niu is with the State Key Laboratory of Rail Traffic Control and Safety, Beijing Jiaotong University, Beijing 100044, China, and also with the National Mobile Communications Research Laboratory, Southeast University, Nanjing 211189, China (e-mail: niuy11@163.com).

B. Ai, R. He and Z. Zhong are with the State Key Laboratory of Rail Traffic Control and Safety, Beijing Jiaotong University, Beijing 100044, China, and also with Beijing Engineering Research Center of High-speed Railway Broadband Mobile Communications, Beijing 100044, China (e-mails: boai@bjtu.edu.cn, ruisi.he@bjtu.edu.cn and zhdzhong@bjtu.edu.cn).

Z. Han is with the Department of Electrical and Computer Engineering in the University of Houston, Houston, TX 77004 USA, and also with the Department of Computer Science and Engineering, Kyung Hee University, Seoul, South Korea, 446-701. (e-mail: zhan2@uh.edu).

N. Wang is with the School of Information Engineering, Zhengzhou University, Zhengzhou 450001, China (e-mail: ienwang@zzu.edu.cn).

X. Su is with the Department of Computer Science, Norwegian University of Science and Technology, 2815 Gjøvik, Norway, and also with the Center of Ubiquitous Computing, University of Oulu, 90570 Oulu, Finland (e-mail:xiang.su@ntnu.no).

to the interruption of wireless links. In order to guarantee user experience, providing reliable network connection is a serious challenge for mm-wave communication.

At present, intelligent reflecting surface (IRS), an innovative and revolutionary technology has developed, which can be used to efficiently improve the system performance [6]. IRS is a low-power passive device that can be widely deployed in indoor ceilings, building surfaces, and even lampposts and walls [7]. Through proper deployment of IRS and intelligent adjustment of beam direction, reliable auxiliary connection can be established. It can help users overcome the influence of block and achieve a significant improvement in spectral efficiency and energy efficiency. Thus, IRS technology has attracted a lot of attentions from academia and industry. Because IRS does not introduce additional noise in the signal reflection process, it has comparative advantages over traditional communication technologies [8] [9].

However, IRS usually does not have radio frequency (RF) links, and consequently the channel cannot be estimated. Moreover, the amounts of reflection elements are usually configured for IRS, and so the estimated channel parameters will increase proportionally as the number of reflection elements increase. Therefore, how to obtain the channel state information (CSI) between the IRS and the BS as well as between the IRS and the MR has become a crucial challenge in the practical application of IRS. In [10], the authors proposed a two-timescale channel estimation framework to exploit the property that the BS-IRS channel is high-dimensional but quasi-static, while the IRS-user (UE) channel is time-varying but low-dimensional. Particularly, to estimate the quasi-static BS-IRS channel, a dual-link pilot transmission scheme was proposed, where the BS transmits downlink pilots and receives uplink pilots reflected by the IRS. As for HSR scenario, the high dynamic fast time-varying channel between the BS beside the track and the MR can be split into the cascade form of BS-IRS channel and IRS-MR channel. The fast time-varying LoS link channel between IRS-MR/BS-MR can be predicted according to the characteristics of high-speed train running along a fixed trajectory [11] [12]. The quasi-static channel between BS-IRS can be obtained by using some advanced channel estimation methods [13] [14]. In addition, the CSI obtained above can also well solve the problem of Doppler shift pre-compensation. In view of the above discussions, the channel estimation is out of the scope of this paper.

At the same time, the IRS passive beam and the BS/MR active beam need to be jointly designed to optimize the end-to-end communication between the MR and the BS. Nevertheless, CSI updates quickly, and the signaling cost of frequently measuring real-time CSI is large in high-speed mobile scenarios. Frequent adjustment of phase amplitude parameters of IRS reflection elements according to real-time CSI in short coherence time also brings a large amount of signaling overhead. As a result, although the perfect CSI can be acquired according to discussed above, it is difficult to achieve rapid and frequent adjustment of IRS parameter matrix in the actual system [15], and so the IRS design based on perfect CSI in high-speed mobile communication system faces serious challenges.Therefore, in this paper, we take both perfect instantaneous CSI and statistical CSI into consideration, which aims to show difference between the two situation and prove the system performance can also be improved with statistical CSI. As for how to obtain the statistical CSI, a transmission frame is composed of a certain number of blocks, and the angle of arrival (AoA)/ angle of departure (AoD) is estimated once in the frame header in this paper. And in the channel estimation phase, the IRS is in the sensing mode and the statistical channel information between the IRS and the BS/MR can be estimated using the dedicated sensors at the IRS and leveraging the pilots and/or data transmitted in both uplink and downlink. Similarly, the statistical channel information between BS and MR can also be estimated. Moreover, the statistical CSI varies more slowly than the instantaneous CSI and can be comparatively easily explored. As the channel estimation is out of the scope of this paper, the detailed discussion is omitted here. The related research studies on how to estimate the channels for IRS-aided systems can be found in [16] [17].

For the purpose of further enhancing the system performance, this paper considers the mm-wave downlink multiple-input multiple-output (MIMO) communication system assisted by IRS in the HSR scenario. Multiple antenna elements are deployed at both the BS and the MR, and the antenna gain is obtained by using beamforming technology. The phase of each reflection element on the IRS is dynamically adjusted to enhance the robustness of the system. In addition, in view of the challenge brought by the uncertainty of the channel, statistical CSI is also employed to jointly design the transceiver beamforming scheme and IRS phase shift matrix. Therefore, in this study, we focus on the average system throughput optimization problem with instantaneous CSI and the average system ergodic capacity maximization problem with statistical CSI respectively. Obviously, the two problems are non-convex thereby challenging to be solved, and so a low-complexity alternate optimization (AO) method is used to obtain the solution. Our contributions are fourfold.

- An IRS-assisted mm-wave HSR communication system model is developed with the aim of improving the system performance, where we symmetrically deploy two IRSs on the lampposts around the BS. Thus, there are both direct link BS-MR and reflect link BS-IRS-MR.
- With instantaneous CSI, the average system throughput maximization problem is formulated by jointly optimizing the transceiver beamforming vector and IRS's phase shift matrix, subjected to the transmitting power constraint and phase shift constraint. Considering that the formulated optimization problem is non-convex, we use the AO method, which iteratively optimizes two seperated sub-problems, i.e., transceiver beamforming vector and phase shift matrix optimizations.
- Given the specificity of the HSR scenario, we also formulate the average system ergodic capacity maximization problem and obtain upper bound of the average system ergodic capacity with statistical CSI. The form of this optimization problem is comparable to the case of instantaneous CSI, and so we utilize the AO method as well to

obtain the optimized transceiver beamforming vector and IRS's phase shift matrix.
- Through simulations under various system parameters, the simulation results show that the system performance of mm-wave HSR communication networks with IRS as well as phase shift optimization has a significant improvement in terms of the average system throughput with instantaneous CSI and the average system ergodic capacity with statistical CSI in comparison with the other two benchmark schemes.

The remainder of the paper is organized as follows. A detailed overview of the related work is predented in Section II. In Section III, the IRS assisted mm-wave HSR communication system model is presented, and the two optimization problems of maximizing the average system throughput with instantaneous CSI and maximizing the average system ergodic capacity with statistical CSI are formulated. The two proposed AO based algorithms are presented in Sections IV and V, respectively. In Section VI, we provide the simulation results under different system parameters. Finally, we draw the conclusions of this paper in Section VII.

II. Related Work

A. Mm-wave communications for HSRs

Key technologies of mm-wave communications for HSRs has attracted extensive attention from academia. Yan *et al.* [18] [19] proposed the control/user plane decoupled network architecture for mm-wave HSR communication systems. In [20], the authors further expanded the network architecture by using mm-wave frequency band (32 GHz). For the purpose of improving the capacity of the system, the authors also deployed multiple antenna elements at the receiving and transmitting and utilized beamforming technology to obtain antenna gain. Song *et al.* [21] further carried out research on key technologies in the HSR mm-wave communication system. Firstly, they proposed a new multiple access scheme based on single carrier technology and orthogonal frequency division multiplexing (OFDM) technology. In addition, they proposed a new architecture using beamforming and spatial multiplexing technology to obtain space division multiplexing gain. Also, the architecture proposed in this paper can alleviate the contradiction between limited spectrum resources and broadband mobile communication business demand. Based on the train position, a dynamic tracking algorithm of beamforming to jointly adjust the width and direction of the beam to maximize the system capacity was proposed in [22]. In addition, the potential application of HSR mm-wave communication, such as railway state detection [23], the mobile edge caching of multimedia service [24], heterogeneous network [25] etc., are using the mm-wave communication to promote the future development and deployment of the intelligent railway mobile communication system. Moreover, the Doppler effect is an important factor that can not be ignored due to the high-speed of HSRs. Fortunately, as the wireless channel is mainly line-of-sight (LoS) in HSR mm-wave communications systems, there is only the Doppler shift [26]. And authors in [27] proposed a scheme which leveraged the continuous location information of the trains to pre-compensate the Doppler shift. Thus, we did not take the Doppler effect into consideration in this paper.

B. IRS-assisted wireless communications

IRS is a new breakthrough technology that integrates amounts of low-cost passive metamaterial elements in a two-dimensional plane and uses programmable software to reconfigure the environment for radio wave propagation. The concept of IRS was first proposed in [8]. The authors studied a multi-input single-output wireless communication system assisted by IRS and found that the network performance can be improved to a great extent by the assistance of IRS. In addition, the signal-to-noise ratio (SNR) of the user is found to have a linear relationship with the square of the number of intelligent reflection elements. In [28], the authors provided a detailed overview on principles, challenges, and opportunities for IRS-assisted wireless communications. Authors in [29] presented an introduction of IRS commonly used models. Moreover, they described a variety of use cases for future communication systems and elaborated how to integrate the IRS technology with current communication systems. The focus of [30] is to reduce mutual interference between cellular link and multiple device-to-device links share the same spectrum so as to improve the system sum rate. To increase the coverage of the mm-wave BS in hotspot areas, unmanned aerial vehicle (UAV) equipped with IRS (UAV-IRS) is used and energy-aware multi-armed bandit (EA-MAB) algorithm is proposed to maximize the achievable data rate while minimizing the energy cost of the UAV flight in, as well as select the next hotspot in the UAV trajectory [31].

C. Beamforming for IRS-assisted wireless communications

Beamforming is an critical issue in wireless systems based on IRSs. First of all, assuming that the perfect CSI is known, many studies on the joint design of the transceiver beamforming and IRS phase shift have been carried out [32]–[34]. In [35], the authors proposed a joint design scheme of continuous digital beamforming for the BSs and discrete analog beamforming for the IRS. Zhang *et al.* [36] did a research on an uplink IRS-assisted communication system, the authors assumed that the IRS phase shifts were limited and they investigated how many phase shifts were enough. In addition, they evaluated the system performance by approximately calculating the achievable data rate.Due to the passive characteristics of IRS, it is difficult to accurately obtain perfect channel information of IRS associated channel [37]. Subsequently, a lot of work has been carried out on channel estimation research for IRS-assisted communication systems under imperfect CSI conditions [16] [17]. As the finite channel training is limited by power, frequency, time, etc., it inevitably produces estimation errors. The phase amplitude parameter design of IRS is closely related to the accuracy of CSI, and the performance of the IRS system is seriously affected by channel estimation errors [9]. To solve this problem, authors in [38] proposed codebook-based phase shifters for mm-wave transmitter and IRS which can avoid estimating their CSI. In addition, the authors jointly optimized the phase shift

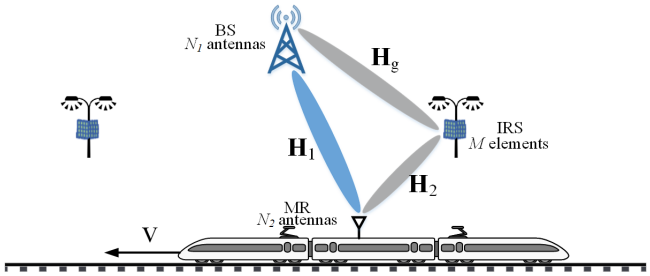

Fig. 1. IRS-assisted mm-wave HSR communication system model.

vectors at both mm-wave BS and IRS by leveraging an online learning approach in the form of a MAB game, which could relax the required beamforming training overhead. Based on this, a nested two-stage Thompson sampling (TS) and upper confidence bound (UCB) algorithms were proposed.

D. IRS-assisted mm-wave HSR communications

As for IRS-assisted mm-wave HSR communication system, Zhang *et al.* [39] provided a detailed survey on challenges, solutions, and future directions for IRS-assisted next generation HSR communication systems. In [40], a novel framework that uses IRS-enabled UAVs was proposed to maximize the system capacity. However, this work assumed that CSI can be perfectly known, which is difficult to achieve in HSR scenario. Given the specificity of the HSR scenario, in [41], a scheme that utilizes statistical CSI to optimize transceiver beamforming vector and IRS phase shift was proposed with the purpose of minimizing the outage probability for the IRS-assisted HSR communication system. In addition, the authors in [42] exploited the benefits of Artificial intelligence (AI) to jointly optimize the transmit beamforming vector at the BS and the phase shift at the IRS. A novel deep reinforcement learning framework which combines long short-term memory (LSTM) and deep deterministic policy gradient (DDPG) was proposed to maximize spectral efficiency with comparatively low time complexity.

From discussions above, we can conclude that there are few IRS studies on MIMO systems, especially the downlink MIMO system lacks effective exploration. Currently, the scenario with single antenna is mainly considered [15], [43]. In addition, there is limited work studying IRS-assisted mm-wave HSR communication system in terms of maximizing the average system throughput with instantaneous CSI and the average system ergodic capacity with statistical CSI.

III. System Overview and Problem Formulation

A. System Model

In this paper, we consider the IRS-assisted mm-wave HSR downlink MIMO communication system as shown in Fig. 1. The train runs in one direction at a uniform speed and the MR is deployed on the roof to avoid penetration loss and reduce frequent group handovers. In addition, the BS and MR are equipped with N_1 and N_2 antennas, respectively. With the aim at improving spectrum efficiency, we symmetrically deploy two IRSs on the lampposts around the BS. In addition, the BS is connected to the controller of each IRS by wire. Assuming that each IRS deploys M reflection elements, the phase/amplitude of each reflection element can be adjusted separately to make the beam in the appropriate direction. According to the location of the train, the BS selects the IRS closest to MR for communication, while the other IRS is regulated by the BS into a sleep state. In our proposed system model, the direct link BS-MR and reflection link BS-IRS-MR exists at the same time. One for communication and the other one for measurement of received signal power. In addition, the two links are at different frequency band, and so there is no interference. In addition, directional antennas are deployed at both the transmitter and the receiver to achieve the high antenna gain by the analog beamforming technique in mm-wave communication systems [44]–[46]. As a result, the signal of the direct link BS-MR and the reflection link BS-IRS-MR have different beam directions, which can be distinguished at the receiving end. And assuming the two links exist at the same time is to conduct switch between the two links and improve the system reliability as well. The switching criteria is based on the received signal power at the MR measured over these two links and will be illustrated in more detail in the following problem formulation part. Furthermore, it is important to note that most of the current schemes studied in other literatures are two links both used for communication at the same time. Although this scheme that both links used for communications can improve the system performance to a greater extent than the scheme proposed in this paper, the receiving signal processing at the MR side is more complex in this way since it needs to add the two links, and the IRS phase shift optimization problem is more complex as well. Consequently, we propose a novel but simple link selection based system model to improve the system performance in terms of the average system throughput and the average system ergodic capacity.

At each time slot t, the transmitting signal $x(t) \in \mathbb{C}$ transmitted by the BS to the MR satisfies $\mathbb{E}\{x(t)\} = 0$ and $\mathbb{E}\left\{x(t)x(t)^H\right\} = 1$. The transmitting beam vector at the BS is denoted as $\mathbf{f}(t) \in \mathbb{C}^{N_1 \times 1}$, and the receiving beam vector at the MR end is denoted as $\mathbf{w}(t) \in \mathbb{C}^{N_2 \times 1}$. The received signal at the MR from the direct link and reflect link are written as $y_1(t) = \mathbf{w}^H(t)\left(\left(\mathbf{H}_1(t)^H\right)\mathbf{f}(t)x(t) + \mathbf{n}(t)\right)$ and $y_2(t) = \mathbf{w}^H(t)\left(\left(\mathbf{H}_2(t)^H\mathbf{\Phi}(t)\mathbf{H}_g(t)\right)\mathbf{f}(t)x(t) + \mathbf{n}(t)\right)$, respectively, where P_T is the transmit power of the BS, $\mathbf{H}_1(t) \in \mathbb{C}^{N_1 \times N_2}, \mathbf{H}_g(t) \in \mathbb{C}^{N_1 \times M}$ and $\mathbf{H}_2(t) \in \mathbb{C}^{M \times N_2}$ represent the channel matrix coefficients between BS-MR, BS-IRS, and IRS-MR, respectively. $\mathbf{n}(t) \sim \mathcal{CN}\left(\mathbf{0}, \sigma^2\mathbf{I}_{N_2}\right)$ indicates the additive Gaussian white noise introduced and its noise power is denoted as σ^2.

We define a diagonal matrix to denote the reflection-coefficients matrix of the IRS which can be expressed as $\mathbf{\Phi} = \mathrm{diag}\left\{\beta_1 e^{j\phi_1}, \cdots, \beta_M e^{j\phi_M}\right\}$, where j represents imaginary unit and $\mathrm{diag}(\cdot)$ represents diagonal matrix function. $\phi = [\phi_1, \cdots, \phi_M]$ denotes the phase shift vector of IRS, $\beta = [\beta_1, \cdots, \beta_M]$ represents the amplitude reflection coefficient vector of IRS, $\phi_m \in [0, 2\pi)$ and $\beta_m \in [0, 1]$ correspond to the phase shift and amplitude of the m-th element of the

IRS, respectively. Usually assuming that the IRS is configured with a constant amplitude value and continuous phase-shift, that is, $\beta_m = 1$ and $|\phi_m|^2 = 1$ [33]. This assumption is also adopted in this paper.

Therefore, the SNR received by the MR of the direct link BS-MR in time slot t $\gamma_1(t)$ can be expressed as

$$\gamma_1(t) = \frac{\left|\mathbf{w}(t)^H \left(\mathbf{H}_1(t)^H\right) \mathbf{f}(t)\right|^2}{\sigma^2}, \tag{1}$$

where $|\cdot|$ is the absolute value of a complex number. Similarly, the SNR received by the MR of the reflect link BS-IRS-MR in time slot t $\gamma_2(t)$ can be expressed as

$$\gamma_2(t) = \frac{\left|\mathbf{w}(t)^H \left(\mathbf{H}_2(t)^H \mathbf{\Phi}(t) \mathbf{H}_\mathbf{g}(t)\right) \mathbf{f}(t)\right|^2}{\sigma^2}. \tag{2}$$

B. Channel Model

In general, especially in China, most rails are paved on viaducts and rural areas, where the wireless channels are mostly LoS [47]. As a result, it is considered that all included links obey the Rician fading model in this paper since LoS components and non-line-of-sight (NLoS) components may exist in practice [41] [48]. In addition, since both BS and IRS are in a static state, the CSI of channel $\mathbf{H}_g$ between the BS and IRS can be perfectly known. The channel model of direct link BS-MR $\mathbf{H}_1$ follows Rician fading, and can be expressed as

$$\mathbf{H}_1 = \sqrt{\frac{\zeta_1}{\zeta_1 + 1}} \bar{\mathbf{H}}_1 + \sqrt{\frac{1}{\zeta_1 + 1}} \tilde{\mathbf{H}}_1, \tag{3}$$

where ζ_1 represents the Rician K-factor of the direct link $\mathbf{H}_1$, $\bar{\mathbf{H}}_1$ represents the LoS component which is determined by the link distance as well as can remain stable within each time slot [49]. $\tilde{\mathbf{H}}_1$ represents the NLoS components. Each element of $\tilde{\mathbf{H}}_1$ is circularly symmetric complex Gaussian (CSCG) distributed with zero mean and variance ${\sigma_1}^2$. It is assumed that the antenna elements at the BS adopt the uniform linear array (ULA) configuration, and $\bar{\mathbf{H}}_1$ can be expressed as

$$\bar{\mathbf{H}}_1 = \mathbf{a}_{MR}\left(\theta_{AoA,1,1}\right) \mathbf{a}_{BS}^H\left(\theta_{AoD,2,1}\right), \tag{4}$$

where $\theta_{AoA,1,1}$,$\theta_{AoD,2,1}$ represents the AoA to the MR and the AoD from the BS, respectively. As the track and real-time location information of the train are known, the transmission distance, AoA and AoD can be calculated.

The link between IRS and MR is also characterized by Rician fading model, which can be expressed as

$$\mathbf{H}_2 = \sqrt{\frac{\zeta_2}{\zeta_2 + 1}} \bar{\mathbf{H}}_2 + \sqrt{\frac{1}{\zeta_2 + 1}} \tilde{\mathbf{H}}_2, \tag{5}$$

where ζ_2 represents the Rician K-factor of the IRS-MR link $\mathbf{H}_2$, $\bar{\mathbf{H}}_2$ represents the LoS component. $\tilde{\mathbf{H}}_2$ represents the NLoS components, whose elements also all satisfy the CSCG distribution with zero mean and variance ${\sigma_2}^2$. The antenna elements of MR are also assumed as ULA configuration, so the expression of the LoS component $\bar{\mathbf{H}}_2$ is similar to (4), which is not described here.

Since IRS can be consisted of amounts of reflecting elements, uniform planar array (UPA) deployment is considered. Moreover, as the CSI of the BS-IRS link can be precisely known in advance, the BS-IRS channel $\mathbf{H}_g$ can be characterized as

$$\begin{aligned} \mathbf{H}_g &= \mathbf{a}_{IRS}\left(\vartheta_{AoA,1,e}, \vartheta_{AoA,1,a}\right) \mathbf{a}_{BS}^H\left(\vartheta_{AoD,2}\right) \\ &= \mathbf{a}_{IRS,a}\left(\vartheta_{AoA,1,a}\right) \otimes \mathbf{a}_{IRS,e}^H\left(\phi_{AoA,1,e}\right) \mathbf{a}_{BS}^H\left(\vartheta_{AoD,2}\right), \end{aligned} \tag{6}$$

where $\otimes$ denotes the Kronecker product, $\vartheta_{\text{AoA},1,e}\left(\vartheta_{\text{AOA},1,a}\right)$, $\vartheta_{AoD,2}$ denote the azimuth (elevation) AoA to the IRS, and the AoD from the BS, of the BS-IRS link, respectively. It is important to note that the LoS part of the BS-MR direct link, $\bar{\mathbf{H}}_1$, and the LoS part of the IRS-MR link, $\bar{\mathbf{H}}_2$, are both dependent on the location of the MR, which varies with the HSR and can be known precisely. Meanwhile the BS-IRS link, $\mathbf{H}_g$, can be precisely known in advance and is stationary.

C. Problem Formulation

From the discussion above, since we assume that the direct link and the reflect link exist at the same time, we define two binary variables a_1 and a_2 to denote which link is used for communication. If $a_1/a_2 = 1$, it means the direct/reflect link is used for communication and the other is used for the received signal power measurement. If the link used for measurement performs better than the link used for communication during a time interval T in terms of average received signal power, the system will switch the former measurement link to the communication link in the next time interval. Taking the example of switching from the direct link to the reflect link, assuming that instantaneous CSI can be acquired, the switching condition mathematical formula can be given by

$$\frac{\sum_{t=1}^{T} \left|\mathbf{w}(t)^H \left(\mathbf{H}(t)^H\right) \mathbf{f}(t)\right|^2 - \sum_{t=1}^{T} \left|\mathbf{w}(t)^H \left(\mathbf{H}_1(t)^H\right) \mathbf{f}(t)\right|^2}{\sum_{t=1}^{T} \left|\mathbf{w}(t)^H \left(\mathbf{H}_1(t)^H\right) \mathbf{f}(t)\right|^2} \geq \xi \tag{7}$$

where $\mathbf{H}(t)^H = \mathbf{H}_2(t)^H \mathbf{\Phi}(t) \mathbf{H}_g(t)$, and ξ is set to prevent frequent handovers between the direct link and reflect link. However, since the instantaneous CSI acquisition will introduce too much overhead, we also consider a more realistic situation, that is instead of maximizing instantaneous channel capacity according to instantaneous CSI, transceiver use statistical CSI to maximize ergodic capacity. The switching condition mathematical formula is similar to (7), except that the statistical CSI is used when calculating the average received signal power, and hence is omitted for simplicity.

In this paper, we focus on maximizing the average system throughput with instantaneous CSI and maximizing the average system ergodic capacity with statistical CSI, along with joint IRS phase shift matrix and transceiver beamforming design, subject to the constraints of the transmit power budget of the BS, IRS constant modulus and only one link is used for communication during a time interval T. Firstly, with instanta-

neous CSI, from the Shannon's formula, the transmission rate of the direct link can be derived as

$$R_1(t) = \log_2\left(1 + \left(\frac{\left|\mathbf{w}(t)^H\left(\mathbf{H}_1(t)^H\right)\mathbf{f}(t)\right|^2}{\sigma^2}\right)\right). \quad (8)$$

Similarly, the transmission rate of the reflect link can be written as

$$R_2(t) = \log_2\left(1 + \left(\frac{\left|\mathbf{w}(t)^H\left(\mathbf{H}_2(t)^H\mathbf{\Phi}(t)\mathbf{H}_g(t)\right)\mathbf{f}(t)\right|^2}{\sigma^2}\right)\right). \quad (9)$$

The average system throughput maximization problem is mathematically formulated as

$$\text{P1}: \max_{\mathbf{w},\mathbf{f},\mathbf{\Phi}} \frac{\int_{t=0}^{2D/v}\left(a_1R_1(t) + a_2R_2(t)\right)dt}{2D/v} \quad (10)$$
$$\text{s.t.} \quad a_1 + a_2 \le 1 \quad (10a)$$
$$||\mathbf{f}||^2 \le P_T, \quad (10b)$$
$$||\mathbf{w}||^2 \le 1, \quad (10c)$$
$$|\phi_m|^2 = 1, \forall m \in \{1,\ldots,M\}, \quad (10d)$$

where D denotes the BS's coverage radius, the speed of the HSR is v, P_T is the transmitting power budget of the BS, $\|\cdot\|$ denotes the Euclidean norm operator.

Then, with statistical CSI, the ergodic capacity of the direct link can be derived as

$$C_{erg}^1(t) = \mathbb{E}\left\{\log_2\left(1 + \frac{\left|\mathbf{w}(t)^H\mathbf{H}_1{}^H(t)\mathbf{f}(t)\right|^2}{\sigma^2}\right)\right\} \quad (11)$$

where $\mathbb{E}\{\cdot\}$ denotes the statistical expectation operator. Similarly, the ergodic capacity of the reflect link can be written as

$$C_{erg}^2(t) = \mathbb{E}\left\{\log_2\left(1 + \frac{\left|\mathbf{w}(t)^H\left(\mathbf{H}_2{}^H(t)\mathbf{\Phi}(t)\mathbf{H}_g(t)\right)\mathbf{f}(t)\right|^2}{\sigma^2}\right)\right\}. \quad (12)$$

The average system ergodic capacity maximization problem is mathematically formulated as

$$\text{P2}: \max_{\mathbf{w},\mathbf{f},\mathbf{\Phi}} \frac{\int_{t=0}^{2D/v}\left(a_1C_{erg}^1(t) + a_2C_{erg}^2(t)\right)dt}{2D/v} \quad (13)$$
$$\text{s.t.} \quad a_1 + a_2 \le 1, \quad (13a)$$
$$||\mathbf{f}||^2 \le P_T, \quad (13b)$$
$$||\mathbf{w}||^2 \le 1, \quad (13c)$$
$$|\phi_m|^2 = 1, \forall m \in \{1,\ldots,M\}. \quad (13d)$$

The average system throughput in P1 depends on the transmission rate of the link which is used for communication in time slot t, and the average system ergodic capacity in P2 is also dependent on the ergodic capacity of the communication link in time slot t. Therefore, we can rewrite P1 and P2 in the following simple form

$$\text{P1-1}: \max_{\mathbf{w},\mathbf{f},\mathbf{\Phi}} \quad a_1R_1(t) + a_2R_2(t)$$
$$\text{s.t.} \quad (10a), (10b), (10c), (10d),$$

$$\text{P2-1}: \max_{\mathbf{w},\mathbf{f},\mathbf{\Phi}} \quad a_1C_{erg}^1(t) + a_2C_{erg}^2(t)$$
$$\text{s.t.} \quad (13a), (13b), (13c), (13d).$$

The optimization problems P1-1 and P2-1 are non-convex problems, which are difficult to be solve with the existing methods. In addition, since the fractional objective function in the P2-1 contains statistical expectation function which needs a lot of calculation [50] when the instantaneous CSI is unknown. Furthermore, due to the constant modulus constraint of IRS, obtaining the optimal IRS phase matrix becomes more complicated.

IV. Average System Throughput Optimization with Instantaneous CSI

To address above-mentioned challenges of solving optimization problems P1-1 and P2-1, we propose an algorithm which is based on the AO theory to iteratively optimize each decision variable while the other variables are fixed. In this section, we will solve P1-1, namely maximizing transmission rate of the link which is used for communication in time slot t with instantaneous CSI. Firstly, we optimize the IRS phase shift matrix $\mathbf{\Phi}$ in IV-A. Then, the beamforming vectors of the BS and the MR are optimized in IV-B and IV-C, respectively. the two binary variables a_1 and a_2 are optimized in IV-D. Finally, we provide convergence and complexity analysis in IV-E

A. Optimization of $\mathbf{\Phi}$

Assuming transceiver beamforming vectors are fixed, $a_1 = 0$ and $a_2 = 1$. Only $\mathbf{\Phi}$ is the decision variable. In addition, $\log(\cdot)$ is strictly concave and increasing over $\mathbb{R}_{++}$. Therefore, P1-1 can be equivalent to the following problem

$$\text{P3-1}: \max_{\mathbf{\Phi}} \quad \left|\mathbf{w}^H\left(\mathbf{H}_2^H\mathbf{\Phi}\mathbf{H}_g\right)\mathbf{f}\right|^2 \quad (14)$$
$$\text{s.t.} \quad |\phi_m|^2 = 1, \forall m \in \{1,\ldots,M\}. \quad (14a)$$

By expanding the objective function in (14), the following equation can be obtained:

$$\left|\mathbf{w}^H\left(\mathbf{H}_2^H\mathbf{\Phi}\mathbf{H}_g\right)\mathbf{f}\right|^2 = \text{Tr}\left(\mathbf{\Phi}^H\mathcal{E}\mathbf{\Phi}\mathcal{G}\right) \quad (15)$$

where $\text{Tr}(\cdot)$ represents the matrix trace function, $\mathcal{E} = \mathbf{H}_2\mathcal{B}\mathbf{H}_2^H$, $\mathcal{G} = \mathbf{H}_g\mathcal{A}\mathbf{H}_g^H$, $\mathcal{A} = \mathbf{f}\mathbf{f}^H$, and $\mathcal{B} = \mathbf{w}\mathbf{w}^H$. It is important to note that all these auxiliary variables have no relation with $\mathbf{\Phi}$. In addition, by using the properties of trace operation, we can get $\text{Tr}\left(\mathbf{\Phi}^H\mathcal{E}\mathbf{\Phi}\mathcal{G}\right) = \boldsymbol{\phi}^H\left(\mathcal{E}\odot\mathcal{G}^T\right)\boldsymbol{\phi}$. Then, (15) can be further equivalently converted to

$$\max_{\boldsymbol{\phi}} \boldsymbol{\phi}^H\left(\mathcal{E}\odot\mathcal{G}^T\right)\boldsymbol{\phi} \triangleq \Gamma(\boldsymbol{\phi}). \quad (16)$$

Problem P3-1 is equivalent to

$$\text{P3-1(a)}: \max_{\boldsymbol{\phi}} \quad \Gamma(\boldsymbol{\phi}) \tag{17}$$

$$\text{s.t.} \quad |\phi_m|^2 = 1, \forall m \in \{1, \ldots, M\}. \tag{17a}$$

Because of the quadratic constant modulus constraint, the optimization problem is non-convex. But it can be transformed as a homogeneous quadratically constrained quadratic program (QCQP). Consequently, the optimal ϕ is solved and the optimal IRS phase matrix $\mathbf{\Phi}$ can be further obtained [8].

B. Optimization of $\mathbf{f}$

With optimized $\mathbf{\Phi}$, given $\mathbf{w}$ and $a_2 = 1$, P1-1 is simplified as

$$\text{P3-2}: \max_{\mathbf{f}} \quad \mathbf{f}^H \mathbf{T}_1 \mathbf{f}$$
$$\text{s.t.} \quad \|\mathbf{f}\|^2 \leq P_T.$$

where $\mathbf{T}_1 = \mathbf{H}^{\mathrm{H}} \mathbf{w} \mathbf{w}^{\mathrm{H}} \mathbf{H}$ and $\mathbf{H} = \mathbf{H}_g^H \mathbf{\Phi}^H \mathbf{H}_2$.

The above problem is a convex problem which is equivalent to

$$\text{P3-2(a)}: \min_{\mathbf{f}} L(\mathbf{f}, u) = -\mathbf{f}^H \mathbf{T}_1 \mathbf{f} + u\left(\|\mathbf{f}\|^2 - P_T\right)$$
$$\text{s.t. } u > 0,$$
$$|\ \mathbf{f}\|^2 \leq P_T.$$

Its Karuch-Kuhn-Tucker (KKT) condition is

$$\nabla_{\mathbf{f}} L(\mathbf{f}, u) = -2\mathbf{T}_1 \mathbf{f} + 2u\mathbf{f} = 0,$$

$$\nabla_u L(\mathbf{f}, u) = \|\mathbf{f}\|^2 - P_T = 0.$$

According to the above KKT conditions, The optimal beamforming vector of problem P3-2 is $\mathbf{f} = {\tau_1}^{\max}\sqrt{P_T}$, where ${\tau_1}^{\max}$ is the eigenvector corresponding to the maximum eigenvalue of matrix $\mathbf{T}_1$.

C. Optimization of $\mathbf{w}$

Similar to problem P3-2, with optimized $\mathbf{\Phi}$, given $\mathbf{f}$ and a_2=1, P1-1 is simplified as

$$\text{P3-3}: \max_{\mathbf{w}} \quad \mathbf{w}^H \mathbf{T}_2 \mathbf{w}$$
$$\text{s.t.} \quad \|\mathbf{w}\|^2 \leq 1,$$

where $\mathbf{T}_2 = \mathbf{H}^{\mathrm{H}} \mathbf{f} \mathbf{f}^{\mathrm{h}} \mathbf{H}$. Then, according to P3-2(a), it can be known that the optimal receiving beamforming vector is ${\tau_2}^{\max}$, where ${\tau_2}^{\max}$ is the eigenvector corresponding to the maximum eigenvalue of the matrix $\mathbf{T}_2$.

D. Optimization of a_1/a_2

With optimized $\mathbf{\Phi}$, given $\mathbf{f}$ and $\mathbf{w}$, the binary variable a_1/a_2 can be determined according to (7), namely if (7) is satisfied, a_2=1, otherwise, a_1=1. The transceiver beamforming optimization of a_1=1 is similar to a_2=1. The only difference is changing $\mathbf{H}$ to $\mathbf{H}_1$. In addition, there is no $\mathbf{\Phi}$ optimization with a_1 = 1. To sum up, the average system throughput optimization problem P1 can be solved by the AO algorithm. The specific execution steps are summarized in Algorithm 1. As shown in Algorithm 1, we randomly generate N independent realizations of beamforming vectors at the BS and MR, and select the best pair $(\mathbf{f}, \mathbf{w})$ with the maximal SNR. Then, we update the transceiver beamforming vectors and phase shift in an alternating manner until the algorithm converges, i.e., the average system throughput difference between two successive iterations is less than a certain threshold.

Algorithm 1 Average system throughput optimization algorithm based on AO

Input:
$\mathbf{H}_g, \mathbf{H}_1, \mathbf{H}_2, \zeta_1, \zeta_2, \sigma_1^2, \sigma_2^2$, i=1 and e=1.
for $t = 1 : 2D/v$ **do**
  repeat
    Randomly generate N independent realizations of beamforming vectors at the BS and MR, and select the best pair $(\mathbf{f}, \mathbf{w})$ with the maximal SNR;
    if $a_2 = 1$ **then**
      Obtain $\mathbf{\Phi}^*(\mathbf{t})$ by solving P3-1 with $\mathbf{\Phi}^*(\mathbf{t}) = \mathrm{diag}\left(\boldsymbol{\phi}^*(t)\right)$;
    end if
    Check convergence of (18). If yes, set $\mathbf{\Phi}^*(\mathbf{t}) = \mathrm{diag}\left(\boldsymbol{\phi}^*(t)\right)$, continue; if not, e=e+1, go to Step 4;
    Obtain $\mathbf{f}^*(\mathbf{t})$ by solving P3-2;
    Obtain $\mathbf{w}^*(\mathbf{t})$ by solving P3-3;
    Determine the binary variable a_1/a_2 by (7);
    Update i=i+1.
  until The increase of the average system throughput between two successive iterations is below a threshold ϵ.
end for
Output:
$\mathbf{\Phi}^*, \mathbf{f}^*, \mathbf{w}^*$ and the average system throughput R.

E. Convergence and Complexity Analysis

1) Convergence: The whole algorithm can be seen as the process by iteratively solving the four subproblems as presented in IV-A, IV-B, IV-C and IV-D. As for subproblem-B and subproblem-C, they are guaranteed to converge to a KKT point of P3-2 and P3-3, i.e., a solution satisfying the KKT conditions of the two problems. In addition, as subproblem-A, we define the objective function of ϕ in inner iteration and outer iteration as F_i and F_o respectively, which are given as follows:

$$\mathrm{F_i}(\phi) = \phi^{\mathrm{H}} \left(\mathcal{E} \odot \mathcal{G}^T\right) \phi,$$

$$\begin{aligned}\mathrm{F_o}(\phi, \mathbf{f}, \mathbf{w}) \ &= a_1 \log_2 \left(1 + \left(\frac{\left|\mathbf{w}^H \left(\mathbf{H}_1{}^H\right) \mathbf{f}\right|^2}{\sigma^2}\right)\right) \\ &\quad + a_2 \log_2 \left(1 + \left(\frac{\left|\mathbf{w}^H \left(\mathbf{H}_2{}^H \mathbf{\Phi} \mathbf{H}_g\right) \mathbf{f}\right|^2}{\sigma^2}\right)\right).\end{aligned}$$

To ensure that the objective function of each inner iteration of the proposed algorithm increases, we check if the following condition is met:

$$\frac{\left|\mathrm{F_i}\left(\phi_{\text{new}}\right) - \mathrm{F_i}\left(\phi_{\text{old}}\right)\right|}{\mathrm{F_i}\left(\phi_{\text{old}}\right)} \leq \epsilon. \tag{18}$$

The outer iteration is checked for convergence by the following condition:

$$\frac{|\mathrm{F_o}\left(\phi_{\text{new}}\,,\mathbf{f}_{\text{new}}\,,\mathbf{w}_{\text{new}}\right)-\mathrm{F_o}\left(\phi_{\text{old}}\,,\mathbf{f}_{\text{old}}\,,\mathbf{w}_{\text{old}}\right)|}{\mathrm{F_o}\left(\phi_{\text{old}}\,,\mathbf{f}_{\text{old}}\,,\mathbf{w}_{\text{old}}\right)}\leq\epsilon \quad (19)$$

By generating N random realizations of beamforming vectors at the BS and MR, and we select the best pair $(\mathbf{f},\mathbf{w})$ with the maximal SNR as the initial point of the phase shift optimization subproblem-A. Note that an increasing value of objective function (10) is guaranteed from Step 4 to Step 13. Furthermore, the objective function (10) has the upper bound since the BS has the power constraint. Therefore, the monotonic convergence of Algorithm 1 is guaranteed.

2) Complexity: In each iteration, selecting the best pair $(\mathbf{f},\mathbf{w})$ with the maximal SNR has a complexity of $\mathrm{O}\left(SN^2\log_2 N\right)$, where S denotes the computational complexity of calculating SNR; updating the ideal phase-shift vector of the IRS by using CVX has a complexity of $\mathrm{O}\left(M^{3.5}\log_2\left(\frac{1}{\varepsilon_1}\right)\right)$, where termination criteria ε_1 determines the accuracy of solving the quadratic programming sub-problem [51] [52]; updating the transceiver beamforming vectors for BS and MR by calculating the eigenvalues of matrix $\mathbf{T_1}$ and $\mathbf{T_2}$ has a complexity of $\mathrm{O}\left(N_1^3\right)$ and $\mathrm{O}\left(N_2^3\right)$, where N_1 and N_2 denotes the number of antennas deployed at the BS and the MR, respectively; determining the binary variable $a1/a2$ has a complexity of $\mathrm{O}\left(B\right)$, where B denotes the computational complexity of calculating (7). To conclude, the complexity of the proposed algorithm is $\mathrm{O}\left(IT\left(SN^2\log_2 N+M^{3.5}\log_2\left(\frac{1}{\varepsilon_1}\right)+N_1^3+N_2^3+B\right)\right)$, where I denotes the number of iterations and $T=2D/v$.

V. Average System Ergodic Capacity Optimization with Statistical CSI

In this section, we solve problem P2-1, namely maximizing ergodic capacity of the link which is used for communication in time slot t with statistical CSI. Similar to IV, the core idea of solving the problem is using the AO algorithm to determine the optimal value of each decision variable iteratively until the system converges.

A. Ergodic Capacity Analysis

Since exact expressions for ergodic capacity are difficult to obtain, a tight and manageable upper bound for ergodic capacity is first derived, and then the upper bound for system ergodic capacity is maximized. According to the Jensen's inequality, the objective function in (12) is upper-bounded as follows

$$\mathbb{E}\left\{\log_2\left(1+\frac{\left|\mathbf{w}^H\mathbf{H}^H\mathbf{f}\right|^2P_T}{\sigma^2}\right)\right\}\leq\log_2\left(1+\frac{\mathbb{E}\left\{\left|\mathbf{w}^H\mathbf{H}^H\mathbf{f}\right|^2\right\}P_T}{\sigma^2}\right), \quad (20)$$

where $\mathbf{H}=\mathbf{H}_g^H\mathbf{\Phi}^H\mathbf{H}_2$, and the egodic capacity of the direct link $C_{erg}^1(t)$ is similarly upper-bounded as (20), just change $\mathbf{H}$ to $\mathbf{H}_1$. Then, we establish an upper bound problem

$$\begin{aligned}\text{P2-1-ub}:\max_{\mathbf{w},\mathbf{f},\mathbf{\Phi}}\ & a_2\mathbb{E}\left\{\left|\mathbf{w}^H\mathbf{H}^H\mathbf{f}\right|^2\right\}+a_1\mathbb{E}\left\{\left|\mathbf{w}^H{\mathbf{H}_1}^H\mathbf{f}\right|^2\right\}\\ &=a_2(a_1)\mu_X^2(\mu_{X,1}^2)+a_2(a_1)\sigma_X^2(\sigma_{X,1}^2)\\ \text{s.t.}\ \ & (13a),(13b),(13c),(13d),\end{aligned}$$

where

$$\begin{aligned}\mu_X(\mu_{X,1}) &=\mathbb{E}\left\{\mathbf{f}^H\mathbf{H}\mathbf{w}(\mathbf{f}^H\mathbf{H}_1\mathbf{w})\right\}\\ &=\mathbf{f}^H\mathbb{E}\{\mathbf{H}(\mathbf{H}_1)\}\mathbf{w}\\ &=\mathbf{f}^H\bar{\mathbf{H}}(\bar{\mathbf{H}}_1)\mathbf{w},\end{aligned}$$

$$\begin{aligned}\sigma_X^2(\sigma_{X,1}^2) &=\mathrm{var}\left\{\mathbf{f}^H\mathbf{H}(\mathbf{H}_1)\mathbf{w}\right\}\\ &=\sum_{i=1}^{N_1}\mathbf{f}_i^2\sum_{j=1}^{N_2}\mathbf{w}_j^2\sigma_{i,j}^2(\sigma_{i,j,1}^2)\\ &=\mathbf{f}^H\mathbf{\Lambda}_1(\mathbf{\Lambda}_{1,1})\mathbf{f}\\ &=\mathbf{w}^H\mathbf{\Lambda}_2(\mathbf{\Lambda}_{2,1})\mathbf{w},\end{aligned}$$

$$\begin{aligned}&\mathbf{\Lambda}_1(\mathbf{\Lambda}_{1,1})=\mathrm{diag}(\vartheta),\\ &(\vartheta)_i=\sum_{j=1}^{N_2}\sigma_{i,j}^2(\sigma_{i,j,1}^2)|\mathbf{w}_j|^2,\forall i\in\{1,\cdots,N_1\},\\ &\mathbf{\Lambda}_2(\mathbf{\Lambda}_{2,1})=\mathrm{diag}(\upsilon),\\ &(\upsilon)_j=\sum_{i=1}^{N_1}\sigma_{i,j}^2(\sigma_{i,j,1}^2)|\mathbf{f}_i|^2,\forall j\in\{1,\cdots,N_2\},\end{aligned}$$

$$\begin{aligned}\sigma_{i,j}^2\left(\sigma_{i,j,1}^2\right) &=\mathrm{var}\left\{[\mathbf{H}]_{i,j}\left([\mathbf{H}]_{i,j,1}\right)\right\}\\ &=\mathrm{var}\left\{\left[\alpha_2{\mathbf{H}_g}^H\mathbf{\Phi}^H\bar{\mathbf{H}}_2\right]_{i,j}\left(\left[\alpha_1\bar{\mathbf{H}}_1\right]_{i,j}\right)\right\}\\ &+\mathrm{var}\left\{\left[\beta_2{\mathbf{H}_g}^H\mathbf{\Phi}^H\tilde{\mathbf{H}}_2\right]_{i,j}\left(\left[\beta_1\tilde{\mathbf{H}}_1\right]_{i,j}\right)\right\}\\ &=\beta_2^2\,\mathrm{var}\left\{\left[{\mathbf{H}_g}^H\mathbf{\Phi}^H\tilde{\mathbf{H}}_2\right]_{i,j}\right\}\left(\beta_1^2\,\mathrm{var}\left\{\left[\tilde{\mathbf{H}}_1\right]_{i,j}\right\}\right)\\ &=\beta_2^2\left\|\mathbf{H}_{g_{(:,i)}}\right\|^2\sigma_2^2\left(\beta_1^2\sigma_1^2\right),\end{aligned}$$

$$\alpha_1=\sqrt{\frac{\zeta_1}{\zeta_1+1}},\alpha_2=\sqrt{\frac{\zeta_2}{\zeta_2+1}},$$

$$\beta_1=\sqrt{\frac{1}{\zeta_1+1}},\beta_2=\sqrt{\frac{1}{\zeta_2+1}},$$

$$\bar{\mathbf{H}}\left(\mathbf{H}_1\right)\triangleq\mathbb{E}\left\{\mathbf{H}\left(\mathbf{H}_1\right)\right\}=\alpha_2{\mathbf{H}_g}^H\mathbf{\Phi}^H\bar{\mathbf{H}}_2\left(\alpha_1\bar{\mathbf{H}}_1\right).$$

B. Optimization of $\mathbf{\Phi}$

Assuming transceiver beamforming vectors are fixed, $a_1=0$ and $a_2=1$. Only $\mathbf{\Phi}$ is the decision variable. Also, σ_X^2 is dependent on $\mathbf{f}$ and $\mathbf{w}$, but non-related to $\mathbf{\Phi}$. This implies that with given $\mathbf{f}$ and $\mathbf{w}$, Problem P2-1-ub equals to the following problem

$$\text{P4-1}:\max_{\mathbf{\Phi}}\quad \mu_X^2=\left|\mathbf{f}^H\bar{\mathbf{H}}\mathbf{w}\right|^2 \quad (21)$$

$$\text{s.t.}\quad |\phi_m|^2=1,\forall m\in\{1,\ldots,M\}. \quad (21a)$$

We can observe that the form of the above problem is similar to problem P3-1 in (14), so we also transform problem P4-1 as a homogeneous QCQP. The steps to solve problem P4-1 are the same as problem P3-1, with changing $\mathbf{H}$ to $\bar{\mathbf{H}}$. Thus, the optimal ϕ is solved and the optimal IRS phase matrix $\mathbf{\Phi}$ can be obtained.

C. Optimization of $\mathbf{f}$

With optimized $\mathbf{\Phi}$, given $\mathbf{w}$ and a_2=1, problem P2-1-ub is simplified as

$$\begin{aligned} \text{P4-2}: \max_{\mathbf{f}} \quad & \mu_X^2 + \sigma_X^2 = \mathbf{f}^H \mathbf{\Psi}_1 \mathbf{f} \\ \text{s.t.} \quad & \|\mathbf{f}\|^2 \leq P_T, \end{aligned}$$

where $\mathbf{\Psi}_1 = \mathbf{\Omega}_1 + \mathbf{\Lambda}_1$, $\mathbf{\Omega}_1 = \bar{\mathbf{H}}^{\mathrm{H}} \mathbf{w} \mathbf{w}^{\mathrm{H}} \bar{\mathbf{H}}$. Thus, the optimal beamforming vector of P4-2 is ${\psi_1}^{\max} \sqrt{P_T}$, where ${\psi_1}^{\max}$ is the eigenvector corresponding to the maximum eigenvalue of the matrix $\mathbf{\Psi}_1$.

D. Optimization of $\mathbf{w}$

Similar to problem P4-2, with optimized $\mathbf{\Phi}$, given $\mathbf{f}$ and a_2=1, problem P2-1-ub is simplified as

$$\begin{aligned} \text{P4-3}: \max_{\mathbf{w}} \quad & \mu_X^2 + \sigma_X^2 = \mathbf{w}^H \mathbf{\Psi}_2 \mathbf{w} \\ \text{s.t.} \quad & \|\mathbf{w}\|^2 \leq 1. \end{aligned}$$

where $\mathbf{\Psi}_2 = \mathbf{\Omega}_2 + \mathbf{\Lambda}_2$, $\mathbf{\Omega}_2 = \bar{\mathbf{H}}^{\mathrm{H}} \mathbf{f} \mathbf{f}^{\mathrm{H}} \bar{\mathbf{H}}$. Then, according to P4-2, it can be known that the optimal receiving beamforming vector $\mathbf{w} = {\psi_2}^{\max}$, where ${\psi_2}^{\max}$ is the eigenvector corresponding to the maximum eigenvalue of the matrix $\mathbf{\Psi}_2$.

E. Optimization of a_1/a_2

With optimized $\mathbf{\Phi}$, given $\mathbf{f}$ and $\mathbf{w}$, the binary variable a_1/a_2 can be determined according to the switching condition which is similar to (7). The transceiver beamforming optimization of a_1=1 is similar to a_2=1, with changing $\bar{\mathbf{H}}$ to $\bar{\mathbf{H}}_1$. Moreover, there is no $\mathbf{\Phi}$ optimization with a_1=1. To sum up, the average system ergodic capacity optimization problem P2 can be solved by the AO algorithm. The specific execution steps are summarized in Algorithm 2.

Algorithm 2 Average system ergodic capacity optimization algorithm based on AO

Input:
Statistical CSI: $\mathbf{H}_g, \bar{\mathbf{H}}_1, \bar{\mathbf{H}}_2, \zeta_1, \zeta_2, \sigma_1^2, \sigma_2^2$, i=1 and e=1
for $t = 1 : 2D/v$ **do**
  repeat
    Randomly generate N independent realizations of beamforming vectors at the BS and MR, and select the best pair $(\mathbf{f}, \mathbf{w})$ with the maximal SNR;
    if $a_2 = 1$ **then**
      Obtain $\mathbf{\Phi}^*(\mathbf{t})$ by solving P4-1 with $\mathbf{\Phi}^*(\mathbf{t}) = \mathrm{diag}\left(\boldsymbol{\phi}^*(t)\right)$;
    end if
    Check convergence of inner iteration which is similar to (18). If yes, set $\mathbf{\Phi}^*(\mathbf{t}) = \mathrm{diag}\left(\boldsymbol{\phi}^*(t)\right)$, continue; if not, e=e+1, go to Step 4;
    Obtain $\mathbf{f}^*(\mathbf{t})$ by solving P4-2;
    Obtain $\mathbf{w}^*(\mathbf{t})$ by solving P4-3;
    Determine the binary variable a_1/a_2 by the switching condition which is similar to (7);
    Update i=i+1.
  until The increase of the average system ergodic capacity between two successive iterations is below a threshold ϵ.
end for
Output:
$\mathbf{\Phi}^*, \mathbf{f}^*, \mathbf{w}^*$ and the average system ergodic capacity C.

VI. Performance Evaluation

A. Simulation Setup

In this section, we simulate the performance of the proposed algorithm and analyze the effects under various system parameters in terms of the average system throughput and average system ergodic capacity to verify the effectiveness and efficiency of the proposed algorithm. Particularly, the transmitting power of the BS P_T is set to be 23 dBm, the horizontal distance between the BS and each IRS d_0 is 100 m, the velocity of the train v is 360 km/h, and the Rician factor ζ_1 and ζ_2 are both set to be 10, if not specified. The switch criteria ξ is set to be 15% in this paper, and it is a variable parameter. On the one hand, if this parameter is set small, the frequent switching between the two link will easily occur. On the other hand, if this parameter is set large, it will make the switch more difficult to trigger, which will reduce the average system throughput or average system ergodic capacity. Therefore, after considering the trade-off between the switching times and system performance, we set ξ as 15% in this paper. Furthermore, we simulate the impact of the switch criteria ξ in the following subsection to better illustrate why 15% is selected in this paper. In addition, the path loss model [53] used in this paper is as follows

$$PL = a_0 + 10 b_0 \log_{10}\left(D_{link}\right),$$

where a_0, b_0 and D_{link} represent the interception, the slope and the distance of the transceiver link, respectively. In [53], the authors provided the detailed parameter settings. Main parameters are summarized in Table I.

TABLE I
SIMULATION PARAMETERS

Parameter	Symbol	Value
Carrier frequency	f	28 GHz
System bandwidth	W	500 MHz
Noise spectral density	N_0	-174 dBm/MHz
BS height	$h_{\mathrm{BS\_height}}$	20 m
MR height	$h_{\mathrm{MR\_height}}$	5 m
Radius of the BS	D	350 m
Number of BS antennas	N_1	32
Number of MR antennas	N_2	8

With the aim at verifying the effectiveness of the **Proposed-algorithm** in this paper, two algorithms used as baseline schemes are as follows:

- **Random Phase Shift** (RPS): where the phase-shift vectors ϕ of the IRS elements are randomly given a value.
- **Without IRS**: where there is no IRS-assisted reflecting link in the system, and transceivers can only communicate through direct channels. However, the beamforming method is used to improve the system performance.

B. Impact of ξ

Fig. 2(a) and Fig. 2(b) depict the system performance of the three schemes in terms of average system throughput and average system ergodic capacity when the switch criteria ξ varies from 5% to 25%. With the switch criteria increasing, the average system throughput and the average system ergodic capacity are both decreasing. That is because if this parameter is set large, it will make the switch more difficult to trigger, which will reduce the system performance. Furthermore, in Fig. 2, the two IRS schemes can both improve the system performance that in comparison with the Without-IRS algorithm. In addition, our proposed algorithm reaches the highest average system throughput compared with the other two baseline schemes. Take ξ=15% as an example, the proposed algorithm has 11.5% and 17.8% performance gain in terms of the average system throughput, respectively. Specifically, when ξ=25%, the performance of the RPS scheme is the same as the Without-IRS scheme since the phase shift is randomly determined without optimization, so there is no switch happened between the two links. However, although the smaller the switch criteria ξ is, the better the system performance will be, the frequent switching between the two links will be easily caused. Take ξ=5% as an example, there are five times switching have occurred while there are only two times when ξ=15% . It is important to note that the switching interval is set to be 1s in this paper, so there are seven times switching occurred at most. Therefore, if ξ is set to be a smaller number, there will be more switching times occurred between the two links. Consequently, after considering the trade-off between the switching times and system performance, 15% is adopted in the following simulation experiments.

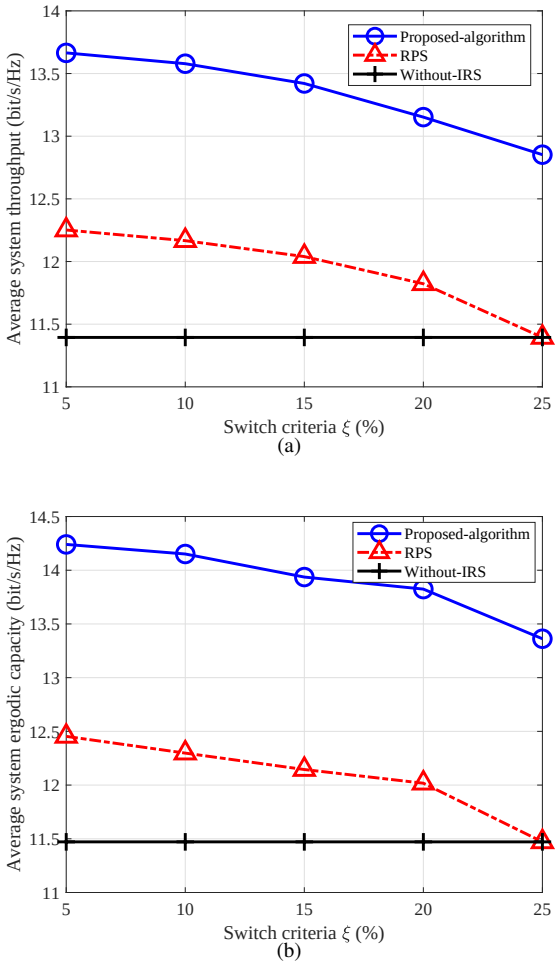

Fig. 2. System performance of the three schemes under different switch criteria values (a) The average system throughput; and (b) The average system ergodic capacity.

C. Average System Throughput Simulation under Instantaneous CSI

1) Impact of P_T: Fig. 3(a) and Fig. 3(b) depict the average system throughput influenced by the transmitting power of the BS which varies from 5 dBm to 30 dBm, the number of reflection elements configured for each IRS and the distance between BS and track $D_{\min}$, respectively. It can be seen from Fig. 3(a) and Fig. 3(b) that as the transmitting power of the BS increases, the signal intensity received by the MR increases and the average system throughput increases. By simulating the performance results of IRS reflection elements number configuration M=64 and M=100, it can be seen that with the increase of the number of reflection elements, the average system throughput also increases. Moreover, it is obvious that the average system throughputs of all the three schemes decrease as $D_{\min}$ increases. In addition, given the transmit power, the number of reflection elements and $D_{\min}$, the average system throughput of without IRS scheme is lower than that of the other two schemes with IRS configuration and our proposed algorithm has the best performance. That is because the two with IRS configuration schemes can choose the one that performs better between direct link BS-MR and reflection link BS-IRS-MR as the communication link, while the Without-IRS scheme only has direct link for communication.

2) Impact of d_0: Fig. 4(a) and Fig. 4(b) depict the relationship between the average system throughput and IRS deployment position under different value of $D_{\min}$, respectively. With the horizontal distance d_0 between the IRS and BS increasing, the average system throughput presents a single-peak trend. When IRS is deployed about 70 m away from the BS, the average system throughput reaches the peak. Actually, this is consistent with the findings in other literature about the IRS deployment, which shows when the IRS is located near the BS or close to the user, the system has the best performance [54]. However, the location of MR is changing all the time in the network. As a result, the best location of the IRS is to be closer to the BS in this paper. The reason why the peak value is not at 0 m is because there is only one IRS at this position while there are two IRSs that are symmetrically deployed about the BS at other positions. We can also observe that as

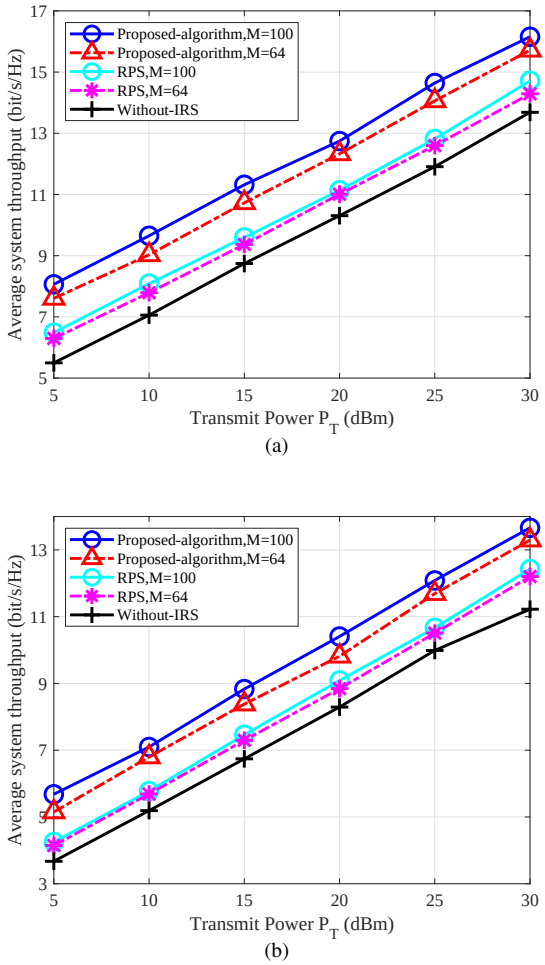

Fig. 3. Average system throughput of the three schemes under different P_T values (a) D_{min}=30; and (b) D_{min}=150.

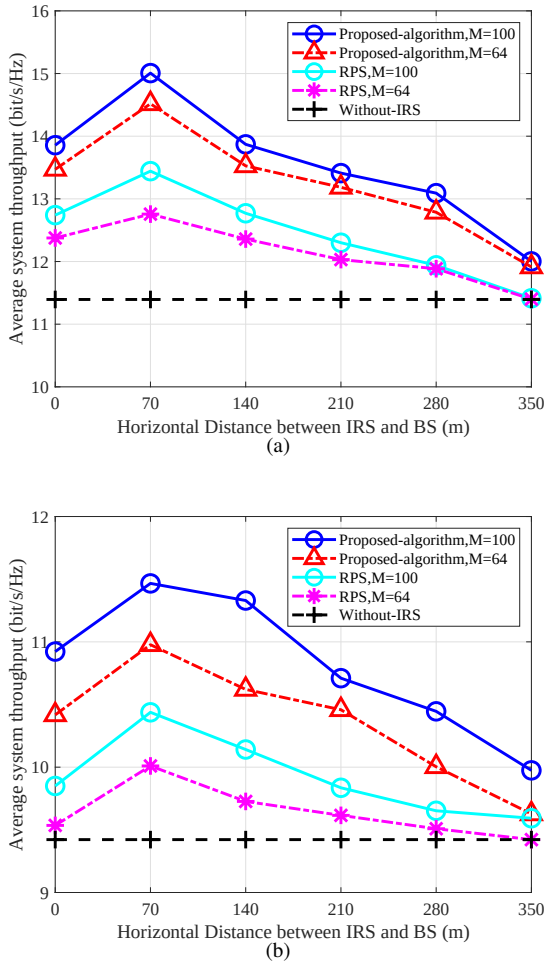

Fig. 4. Average system throughput of the three schemes under different d_0 values (a) D_{min}=30; and (b) D_{min}=150.

$D_{\min}$ increasing, the average system system throughputs of all the three schemes decrease. The above discussed observations can provide experimental guidance for the proper deployment of the IRS to improve system performance. Furthermore, in Fig. 3, it is obvious that in comparison with the Without-IRS algorithm, the two IRS schemes significantly improve the system performance in terms of average system throughput. In addition, our proposed algorithm reaches the highest average system throughput compared with the other two baseline schemes. Take $d_0 = 70$, $M = 100$, $D_{\min} = 30$ as an example, the proposed algorithm has 11.6% and 31.6% performance gain, respectively. Specifically, when IRS is deployed at the edge of the cell, the performance of the RPS scheme is close to the Without-IRS scheme since the phase shift is randomly determined without optimization. Therefore, due to the link selection is involved in our proposed system model, the performance improvement of the RPS scheme is not enough to trigger link switching, so the performance of this scheme reaches the case of Without-IRS at the cell-edge scenario.

D. Average System Ergodic Capacity Simulation under Statistical CSI

1) Impact of M: Fig. 5(a) and Fig. 5(b) depict the system performance of the three schemes under different value of $D_{\min}$ in terms of average system ergodic capacity while the number of reflection elements configured by IRS is varied from 50 to 300, respectively. As the number of reflection elements of IRS increase, the reflect channel is remarkably improved and the average system ergodic capacities of the two IRS schemes increase, while the Without-IRS scheme remains unchanged. Specifically, the proposed algorithm has the highest average system ergodic capacity, while the performance of the RPS scheme is lower than the proposed Algorithm 2 based on AO since the RPS scheme can not guarantee the phase shift ϕ is optimal, indicating that the proposed algorithm improves the system performance to a great extent in terms of average ergodic capacity. Take $M = 200$, $D_{\min} = 30$ as an example, in comparison with the RPS scheme and the Without-IRS scheme, the proposed algorithm has 14.6% and 50.4% performance gain, respectively.

2) Impact of ζ_1: Fig. 6(a) and Fig. 6(b) depict the system performance of the three schemes under different value of $D_{\min}$ in terms of average system ergodic capacity when the Rician factor varies from 0 to 30, respectively. Rician factor is a key parameter to characterize channel quality, and represents

This article has been accepted for publication in IEEE Transactions on Vehicular Technology. This is the author's version which has not been fully edited and content may change prior to final publication. Citation information: DOI 10.1109/TVT.2022.3233066

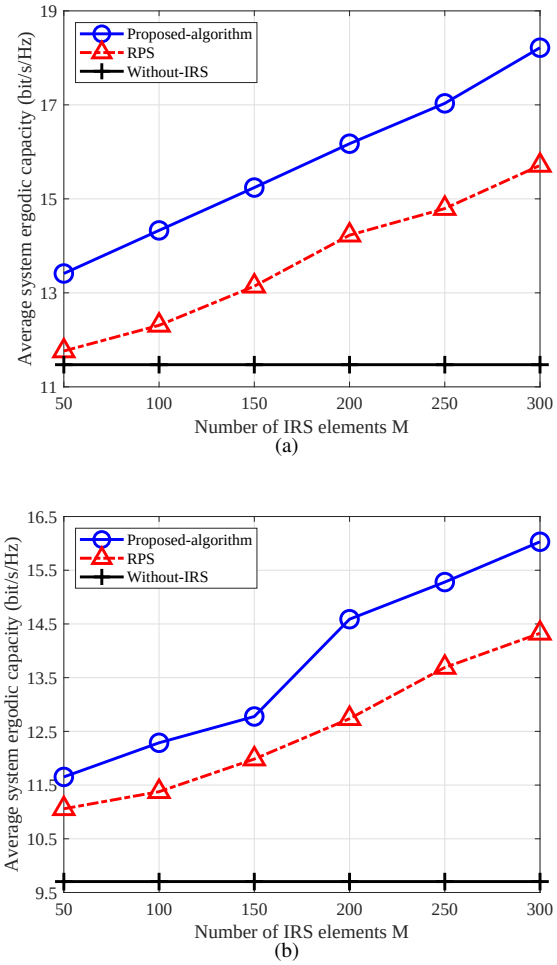

Fig. 5. Average system ergodic capacity of the three schemes under different numbers of IRS reflecting elements (a) D_{min}=30; and (b) D_{min}=150.

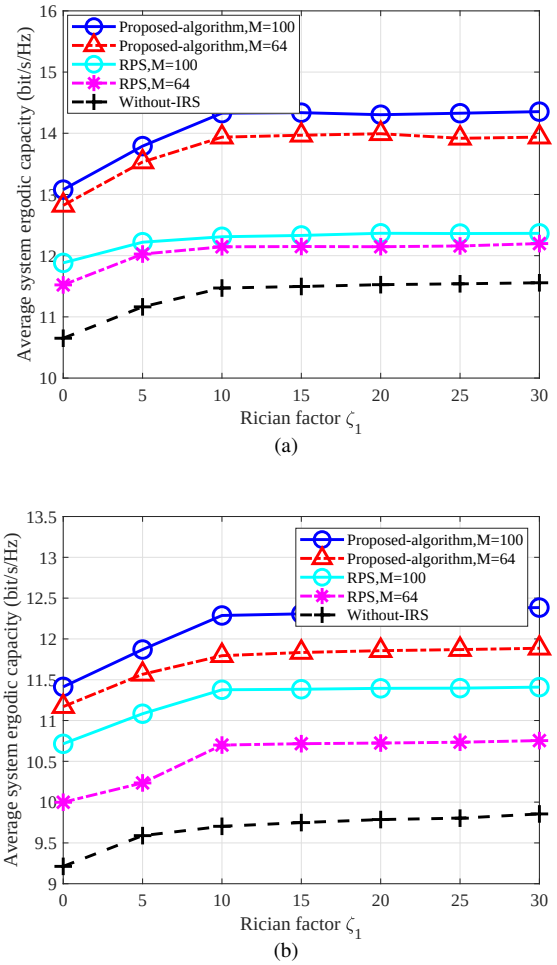

Fig. 6. Average system ergodic capacity of the three schemes under different ζ_1 values (a) D_{min}=30; and (b) D_{min}=150.

the strong and weak ratio between LoS component and NLoS component. The larger the Rician factor is, the stronger the LoS component is and the better the channel quality is. In this paper, it is assumed that the Rician factor of the BS-MR direct channel is the same as the IRS-MR reflect channel, i.e., ζ_1=ζ_2. When $\zeta_1 \to \infty$, it indicates that the NLoS component in the channel can be ignored. When large-scale shadow fading is not considered, the channel coefficient of LoS component remains unchanged in a single time slot, which is a deterministic channel. When ζ_1=0, there is no LoS component in the system and it is Rayleigh channel. From Fig. 5, we can observe that as the Rician factor increases, the average system ergodic capacities of all the three schemes start to increase and then reaches a comparably stable value when ζ_1 equals to 10. To sum up, the algorithm proposed in this paper has a better performance than the other two baseline schemes.

VII. Conclusions

IRS is a new breakthrough technology that is utilized to efficiently enhance the system performance. In this paper, we focus on the IRS assisted mm-wave HSR communication system. Two separated sub-problems, the transceiver beamforming vector and IRS phase shift optimization problems, are formulated respectively to maximize average system throughput with instantaneous CSI and maximize average system ergodic capacity with statistical CSI. The two optimization problems are constrained by transmitting power and constant amplitude modulus. Since the constraints of the decision variables are independent from each other, the AO algorithm is used to solve the two optimization problems. Finally, numerical results have proved that the systems that deploy IRS can increase system capacity while reducing power consumption, and we also observe that the distance between the BS and IRS has great influence on the system performance, which can be used to guide the IRS deployment. In the future work, we will adopt the time-varying 3D Saleh-Valenzuela channel model and take outdated CSI into account to make our study more practical.

References

[1] B. Ai, A. F. Molisch, M. Rupp and Z. Zhong, "5G key technologies for smart railways," *Proceedings of the IEEE*, vol. 108, no. 6, pp. 856-893, Jun. 2020.

[2] D. Fan, Z. Zhong, G. Wang, and F. Gao, "Doppler shift estimation for high-speed railway wireless communication systems with large-scale linear antennas," in *International Workshop on High Mobility Wireless Communications (HMWC)*, Xian, China, pp. 96-100, Oct. 2015.

[3] Y. Lu, J. Qi, F. Hu, and H. Peng, "Application of millimeter wave communication in high-speed railway passenger services," *Railway Signalling & Communication*, vol. 54, no. 5, pp. 50–53, May 2018.

[4] J. O. Sanchez and J. I. Alonso, "A two-hop MIMO relay architecture using LTE and millimeter wave bands in high-speed trains," *IEEE Transactions on Vehicular Technology*, vol. 68, no. 3, pp. 2052–2065, Mar. 2019.

[5] S. Rangan, T. S. Rappaport, and E. Erkip, "Millimeter wave cellular wireless networks: Potentials and challenges," *Proceedings of the IEEE*, vol. 102, no. 3, pp. 366–385, Mar. 2014.

[6] M. D. Renzo et al., "Smart radio environments empowered by reconfigurable AI meta-surfaces: An idea whose time has come," *EURASIP Journal on Wireless Communications and Networking*, vol. 2019, no. 1, pp. 1–20, May 2019.

[7] S. Gong et al., "Toward Smart Wireless Communications via Intelligent Reflecting Surfaces: A Contemporary Survey," *IEEE Communications Surveys Tutorials*, vol. 22, no. 4, pp. 2283–2314, Jun. 2020.

[8] Q. Wu and R. Zhang, "Intelligent Reflecting Surface Enhanced Wireless Network via Joint Active and Passive Beamforming," *IEEE Transactions on Wireless Communications*, vol. 18, no. 11, pp. 5394–5409, Nov. 2019.

[9] C. Huang et al., "Reconfigurable Intelligent Surfaces for Energy Efficiency in Wireless Communication ," *IEEE Transactions on Wireless Communications*, vol. 18, no. 8, pp. 4157–4170, Aug. 2019.

[10] C. Hu, L. Dai, S. Han and X. Wang, "Two-Timescale Channel Estimation for Reconfigurable Intelligent Surface Aided Wireless Communications," *IEEE Transactions on Communications*, vol. 69, no. 11, pp. 7736–7747, Nov. 2021.

[11] T. Li, H. Tong, Y. Xu, X. Su and G. Qiao, "Double IRSs Aided Massive MIMO Channel Estimation and Spectrum Efficiency Maximization for High-Speed Railway Communications," *IEEE Transactions on Vehicular Technology*, vol. 71, no. 8, pp. 8630-8645, Aug. 2022.

[12] L. Yan, X. Fang, L. Hao and Y. Fang, "A Fast Beam Alignment Scheme for Dual-Band HSR Wireless Networks," *IEEE Transactions on Vehicular Technology*, vol. 69, no. 4, pp. 3968–3979, Apr. 2020.

[13] Liu S, Gao Z, Zhang J, et al., "Deep denoising neural network assisted compressive channel estimation for mmWave intelligent reflecting surfaces," *IEEE Transactions on Vehicular Technology*, vol. 69, no. 8, pp. 9223–9228, Aug. 2020.

[14] S. Lim, S. Kim, B. Shim and J. W. Choi, "Efficient Beam Training and Sparse Channel Estimation for Millimeter Wave Communications Under Mobility," *IEEE Transactions on Communications*, vol. 68, no. 10, pp. 6583–6596, Oct. 2020.

[15] L. You et al., "Reconfigurable Intelligent Surfaces-Assisted Multiuser MIMO Uplink Transmission with Partial CSI," *IEEE Transactions on Wireless Communications*, vol. 20, no. 9, pp.5613–5627, Sept. 2021.

[16] C. You, B. Zheng and R. Zhang, "Channel Estimation and Passive Beamforming for Intelligent Reflecting Surface: Discrete Phase Shift and Progressive Refinement," *IEEE Journal on Selected Areas in Communications*, vol. 38, no. 11, pp. 2604-2620, Nov. 2020.

[17] Z. Wang, L. Liu and S. Cui, "Channel Estimation for Intelligent Reflecting Surface Assisted Multiuser Communications: Framework, Algorithms, and Analysis," *IEEE Transactions on Wireless Communications*, vol. 19, no. 10, pp. 6607-6620, Oct. 2020.

[18] L. Yan and X. Fang, "Decoupled Wireless Network Architecture for High-Speed Railway ," in *International Workshop on High Mobility Wireless Communications (HMWC)*, Shanghai, China, pp. 96–100, Nov. 2013.

[19] L. Yan, X. Fang and Y. Fang, "Stable Beamforming with Low Overhead for C/U-Plane Decoupled HSR Wireless Networks," *IEEE Transactions on Vehicular Technology*, vol. 67, no. 7, pp. 6075–6086, Jul. 2018.

[20] H. Song, X. Fang and Y. Fang, "Millimeter-Wave Network Architectures for Future High-Speed Railway Communications: Challenges and Solutions," *IEEE Wireless Communications*, vol. 23, no. 6, pp. 114–122, Dec. 2016.

[21] M. Gao et al., "Dynamic mmWave Beam Tracking for High-Speed Railway Communications," in *IEEE Wireless Communications and Networking Conference Workshops (WCNCW)*, Barcelona, Spain, pp. 278-283, Apr. 2018.

[22] L. Yan, X. Fang, L. Hao and Y. Fang, "Safety-Oriented Resource Allocation for Space-Ground Integrated Cloud Networks of High-Speed Railways," *IEEE Journal on Selected Areas in Communications*, vol. 38, no. 12, pp. 2747–2759, Dec. 2020.

[23] L. Yan et al., "An mmWave Wireless Communication and Radar Detection Integrated Network for Railways," in *IEEE Vehicular Technology Conference (VTC Spring)*, Nanjing, China, May 2016.

[24] M. Gao et al., "Edge Caching and Content Delivery with Minimized Delay for Both High-Speed Train and Local Users," in *IEEE Global Communications Conference (GLOBECOM)*, Waikoloa, HI, USA, Dec. 2019.

[25] Y. Hu, H. Li, Z. Chang and Z. Han, "Scheduling Strategy for Multimedia Heterogeneous High-Speed Train Networks," *IEEE Transactions on Vehicular Technology*, vol. 66, no. 4, pp. 3265-3279, Apr. 2017.

[26] V. Va, X. Zhang, and R. W. Heath, "Beam switching for millimeter wave communication to support high speed trains," in *IEEE Vehicular Technology Conference (VTC-Fall)*, Boston, MA, USA, Sept. 2015.

[27] J. Talvitie, T. Levanen, M. Koivisto, T. Ihalainen, K. Pajukoski, and M. Valkama, "Positioning and location-aware communications for modern railways with 5G new radio," *IEEE Communications Magazine*, vol. 57, no. 9, pp. 24–30, Sept. 2019.

[28] M. A. Elmossallamy et al., "Reconfigurable Intelligent Surfac-es for Wireless Communications: Principles Challenges and Opportunities", *IEEE Transactions on Cognitive Communications and Networking*, vol. 6, no. 3, pp. 990-1002, Sept. 2020.

[29] H. Zhang, B. Di, L. Song and Z. Han, "Recongurable Intelligent Surface-Empowered 6G," *Springer*, 2021.

[30] Y. Chen et al., "Reconfigurable Intelligent Surface Assisted Device-to-Device Communications," *IEEE Transactions on Wireless Communications*, vol. 20, no. 5, pp. 2792-2804, May 2021.

[31] E. M. Mohamed, S. Hashima and K. Hatano, "Energy Aware Multiarmed Bandit for Millimeter Wave-Based UAV Mounted RIS Networks," *IEEE Wireless Communications Letters*, vol. 11, no. 6, pp. 1293–1297, Jun. 2022.

[32] C. Pan et al., "Intelligent Reflecting Surface Aided MIMO Broadcasting for Simultaneous Wireless Information and Power Transfer," *IEEE Journal on Selected Areas in Communications*, vol. 38, no. 8, pp. 1719-1734, Aug. 2020.

[33] Q. Wu and R. Zhang, "Joint Active and Passive Beamforming Optimization for Intelligent Reflecting Surface Assisted SWIPT Under QoS Constraints," *IEEE Journal on Selected Areas in Communications*, vol. 38, no. 8, pp. 1735-1748, Aug. 2020.

[34] G. Zhou et al., "Intelligent Reflecting Surface Aided Multigroup Multicast MISO Communication Systems ," *IEEE Transactions on Signal Processing*, vol. 68, pp. 3236-3251, Apr. 2020.

[35] B. Di et al., "Hybrid beamforming for reconfigurable intelligent surface based multi-user communications: Achievable rates with limited discrete phase shifts," *IEEE Journal on Selected Areas in Communications*, vol. 38, no. 8, pp. 1809-1822, Aug. 2020.

[36] H. Zhang, B. Di, L. Song and Z. Han, "Reconfigurable Intelligent Surfaces Assisted Communications With Limited Phase Shifts: How Many Phase Shifts Are Enough?," *IEEE Transactions on Vehicular Technology*, vol. 69, no. 4, pp. 4498-4502, Apr. 2020.

[37] H. Guo, Y. Liang, J. Chen and E. G. Larsson, "Weighted Sum-Rate Maximization for Reconfigurable Intelligent Surface Aided Wireless Networks ," *IEEE Transactions on Wireless Communications*, vol. 19, no. 5, pp. 3064-3076, May 2020.

[38] E. M. Mohamed, "Two-Stage Multiarmed Bandit for Reconfigurable Intelligent Surface Aided Millimeter Wave Communications," *Sensors*, vol. 22, no. 6, pp. 2179–2196, Mar. 2022.

[39] J. Zhang et al., "RIS-Aided Next-Generation High-Speed Train Communications: Challenges, Solutions, and Future Directions," *IEEE Wireless Communications*, vol. 28, no. 6, pp. 145-151, Dec. 2021.

[40] Y. M. Park, Y. K. Tun, Z. Han and C. S. Hong, "Trajectory Optimization and Phase-Shift Design in IRS-Assisted UAV Network for Smart Railway," *IEEE Transactions on Vehicular Technology*, Early Access, 2022.

[41] M. Gao et al., "IRS-Assisted High-Speed Train Communications: Outage Probability Minimization with Statistical CSI," in *IEEE International Conference on Communications (ICC)* , Montreal, QC, Canada, Jun. 2021.

[42] J. Xu and B. Ai, "When mmWave High-Speed Railway Networks Meet Reconfigurable Intelligent Surface: A Deep Reinforcement Learning Method," *IEEE Wireless Communications Letters*, vol. 11, no. 3, pp. 533–537, Mar. 2022.

[43] Y. Han et al., "Large Intelligent Surface-Assisted Wireless Communication Exploiting Statistical CSI," *IEEE Transactions on Vehicular Technology*, vol. 68, no. 8, pp. 8238-8242, Aug. 2019.

[44] J. Wang et al., "Beam codebook based beamforming protocol for multi-Gbps millimeter-wave WPAN systems," *IEEE Journal on Selected Areas in Communications*, vol. 27, no. 8, pp. 1390-1399, Oct. 2009.

[45] Y. Tsang, A. Poon, and S. Addepalli, "Coding the beams: Improving beamforming training in mmWave communication system," in *IEEE Global Communications Conference (GLOBECOM)*, Houston, TX, USA, Dec. 2011.

[46] Z. Xiao, X. Xia, D. Jin, and N. Ge, "Iterative eigenvalue decomposition and multipath-grouping Tx/Rx joint beamformings for millimeterwave communications," *IEEE Transactions on Wireless Communications*, vol. 14, no. 3, pp. 1595-1607, Mar. 2015.

[47] L. Liu et al., "Position-basedmodeling for wireless channel on high-speed railway under a viaduct at 2.35 GHz," *IEEE Journal on Selected Areas in Communications*, vol. 30, no. 4, pp. 834–845, May 2012.

[48] Y. Cai, M. -M. Zhao, K. Xu and R. Zhang, "Intelligent Reflecting Surface Aided Full-Duplex Communication: Passive Beamforming and Deployment Design," *IEEE Transactions on Wireless Communications*, vol. 21, no. 1, pp. 383–397, Jan. 2022.

[49] Y. Zhang and L. Dai, "A closed-form approximation for uplink average ergodic sum capacity of large-scale multi-user distributed antenna systems," *IEEE Transactions on Vehicular Technology*, vol. 68, no. 2, pp. 1745-1756, Feb. 2019.

[50] Y. Lu et al., "Global Energy Efficiency in Secure MISO SWIPT Systems with Non-Linear Power-Splitting EH Model," *IEEE Journal on Selected Areas in Communications*, vol. 37, no. 1, pp. 216-232, Jan. 2019.

[51] Z. Luo et al., "Semidefinite Relaxation of Quadratic Optimization Problems," *IEEE Signal Processing Magazine*, vol. 27, no. 3, pp. 20–34, May 2010.

[52] Helmberg et al., "An Interior-Point Method for Semidefinite Programming," *SIAM Journal on Optimization*, vol. 6, no. 24, pp. 342–361, May 1996.

[53] D. He et al., "Channel Measurement, Simulation, and Analysis for High-Speed Railway Communications in 5G Millimeter-Wave Band," *IEEE Transactions on Intelligent Transportation Systems*, vol. 19, no. 10, pp. 3144-3158, Oct. 2018.

[54] M. Almekhlafi, M. A. Arfaoui, M. Elhattab, C. Assi and A. Ghrayeb, "Joint Resource Allocation and Phase Shift Optimization for RIS-Aided eMBB/URLLC Traffic Multiplexing," *IEEE Transactions on Communications*, vol. 70, no. 2, pp. 1304–1319, Feb. 2022.